Weld Cracking and Solidification Behavior of Titanium Alloys

Cracking of Ti-alloys depends strongly on microsegregation, determined by the solid-state back-diffusion of solute elements during solidification

BY H. INOUE AND T. OGAWA

ABSTRACT. The weld solidification cracking behavior of three different Ti-alloys was investigated using the Varestraint test. Ti-6Al-4V weld metal did not crack up to 8.3% augmented strain, while cracking was significant over 0.5% augmented strain in Ti-6Al-6V-2Sn and Ti-15V-3Al-3Cr-3Sn weld metal. Marked microsegregation of V, Fe, Cr and/or Cu to dendrite boundaries of each solidification microstructure was confirmed by the tin-quenching method. According to our measurements, the diffusion rate of the solute elements in Ti-6Al-4V alloy was one order of magnitude larger than that in the other two alloys. Hence, any microsegregation occurring in Ti-6Al-4V weld metal during solidification was not significant due to the large solute back-diffusion in the solid, and the dispersed at an early stage of cooling after solidification. On the other hand, any microsegregation that occurred in the other two alloy welds during solidification was very noticeable due to the much smaller back-diffusion of solute elements in the solid, and the fact that it largely remained in ambient temperature owing to the slower solute diffusivity. Solute diffusion rates were determined by experiment using special diffusion couples. As a consequence of microsegregation, the solidification temperature range of Ti-6Al-6V-2Sn and Ti-15V-3Al-3Cr-3Sn alloys would be great, thus forming a residual low-melting liquid film, that resulted in cracks.

H. INOUE and T. OGAWA are with Steel Research Laboratory, Nippon Steel Corp, Shintomi, Futtsu, Chiba, Japan.

Introduction

Due to their high strength-to-weight ratio combined with excellent elevated-temperature properties and good corrosion resistance, Ti-alloys have been used for a wide range of aerospace, marine, and chemical applications. Welding offers an efficient and often cost-effective means of fabricating large structural assemblies. Although Ti-alloys are generally considered to have good weldability with attractive weld properties, several previous studies have indicated that alloys such as Ti-6Al-4V (Ref. 1), Ti-6Al-6V-2Sn (Ref. 2), Ti-3Al-13V-11Cr (Ref. 2), Ti-6Al-2Nb-1Ta-0.8Mo (Ref. 3), and Ti-5.5Al-3.5Sn-3Zr-1Nb-0.25Mo-0.3Si (Ref. 4) are susceptible to weld cracking. It is well established that weld solidification cracking is closely related to nonequilibrium solidification behavior (Refs. 2, 4–7), which leads to microsegregation. Since Ti-alloys solidify as a primary β single phase of a bcc structure, it is technically not always easy to exhibit the solidification microstructure. Hence, the solidification behavior in terms of the element distribution coefficient, microsegregation, and diffusion is still not well understood. The objective of this study was to investigate the solidification behavior and clarify the relationship between solidification cracking and solute segregation.

KEY WORDS

Cracking Behavior
Titanium Alloys
Solidification
Microsegregation
Dendrite Boundaries
Element Diffusivity
Tin Quenching
Aerospace Industry
Marine Applications
Chemical Industry

Experimental Procedure

The chemical compositions of the three Ti-alloy plates studied are shown in Table 1, including two α–β alloys, Ti-6Al-4V and Ti-6Al-6V-2Sn, and a β alloy, Ti-15V-3Al-3Cr-3Sn. The solidification cracking susceptibility of these alloys was examined by the trans-Varestraint test, which is presented schematically in Fig. 1. The specimens, 6 x 100 x 80 mm (0.24 x 4 x 3.1 in.), were degreased with acetone. Welding was performed autogenously using a bead-on-plate weld, made at 100 A and 15 V with a travel speed of 1.66 mm/s (4 in./min) in Ar gas shielding by the gas tungsten arc welding (GTAW) process. As illustrated in Fig. 1, an augumented strain was applied by dropping the yokes at B when the molten weld pool was moving from A to C during welding. The strain was increased from 0.5 to 8.3% by changing the bending radius. The cracking susceptibility was determined by measuring the total and maximum crack lengths in the fusion-zone at each strain level. The solidification microstructures were exhibited by the tin-quenching method, in

Table 1 — Chemical Compositions of Test Materials (wt-%)

Alloy	Al	V	Sn	Cr	Cu	Fe	O	N	C	H	Ti
Ti-6Al-4V	6.46	4.22	—	—	—	0.22	0.12	0.01	0.01	0.0011	Bal.
Ti-6Al-6V-2Sn	5.47	5.70	1.96	—	0.75	0.75	0.18	0.01	0.01	0.0019	Bal.
Ti-15V-3Al-3Cr-3Sn	2.90	15.30	2.98	3.03	—	0.21	0.13	0.01	0.01	0.0078	Bal.

Table 2 — Solute Element Concentration at Hot-Crack and on Fractured Surfaces Obtained by AES Spectra (wt-%)

Alloy	Location	Al	V	Cr	Sn	Ti
Ti-6Al-6V-2Sn	Solidification cracking surface	8.80	6.71	—	0.08	84.41
	Ductile fractured surface	9.02	5.78	—	0.30	84.90
Ti-15V-3Al-3Cr-3Sn	Solidification cracking surface	4.52	20.33	3.69	2.35	69.11
	Ductile fractured surface	5.83	16.60	2.50	2.90	72.17

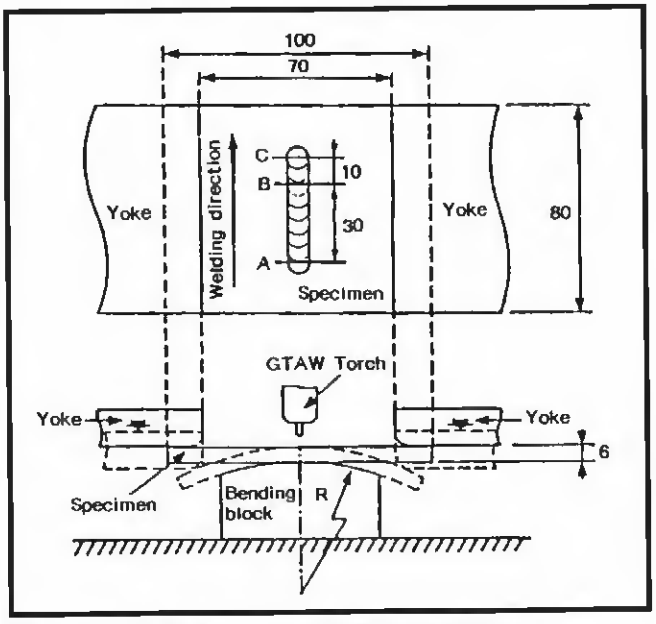

Fig. 1 — Schematic appearance of trans-Varestraint test.

which a large amount of molten tin (573 K) was poured on the moving molten pool during GTA welding. The cooling rate during tin quenching was estimated at over 10^4 K/s from the measurement of the subgrain size at the solidification front (Ref. 8). The composition profiles in the solidification microstructure were examined by an electron probe microanalyzer (EPMA), a computer-aided microanalyzer (CMA), and an auger electron spectroscope (AES).

In order to determine the diffusivity of the solute elements in Ti-alloys, the solute distribution was investigated by studying diffusion welding between Ti-alloy and Type 444 ferritic stainless steel with 0.004C-19Cr. The specimen size of the bonding test was 10-mm diameter x 6-mm thickness (0.4 x 0.24 in.) for the Ti-alloys and 10-mm diameter x 20-mm thickness (0.4 x 0.8 in.) for the stainless steel. The specimen surfaces were ground with emery paper to No. 600 grit and degreased with acetone. The bonding test was conducted at a pressure of 1.5 N/mm^2 and at temperatures of 1273, 1293 and 1323 K for 1800 s in a vacuum of 10^{-4} Torr. The diffusion rates of solute elements were calculated by using measured solute concentrations in the vertical direction to the bonded-joint surfaces. The diffusion welding between commercially pure titanium and the ferritic stainless steel was also studied.

Results and Discussion

Solidification Cracking

Figure 2 shows the maximum and total crack lengths of the fusion zone in the Ti-alloys for trans-Varestraint tests. Ti-6Al-4V weld metal did not crack at all, while Ti-6Al-6V-2Sn and Ti-15V-3Al-3Cr-3Sn cracked over an augumented strain of 0.5%. The crack lengths increased with strain, and the crack length of Ti-15V-3Al-3Cr-3Sn weld metal was larger than that of Ti-6Al-6V-2Sn at every strain level. As shown in Fig. 3, the cracks occurred predominantly along dendritic cell boundaries (b) during solidification, but partly initiated at and propagated along primary β grain boundaries (a). The cracking behavior was similar in both alloys. Figure 4 shows the crack surfaces of Ti-15V-3Al-3Cr-3Sn weld metal, where the solidification front, *i.e.*, the higher temperature side, is to the left. Clear dendritic cell structures at the higher temperature region of A and flat terrace-like features of C in the lower temperature region were observed. The crack surfaces, as a whole, exhibited the predominantly smooth appearance of a liquid vestige. This morphology shows that a residual liquid film played an important role in the cracking mechanism (Ref. 9). The

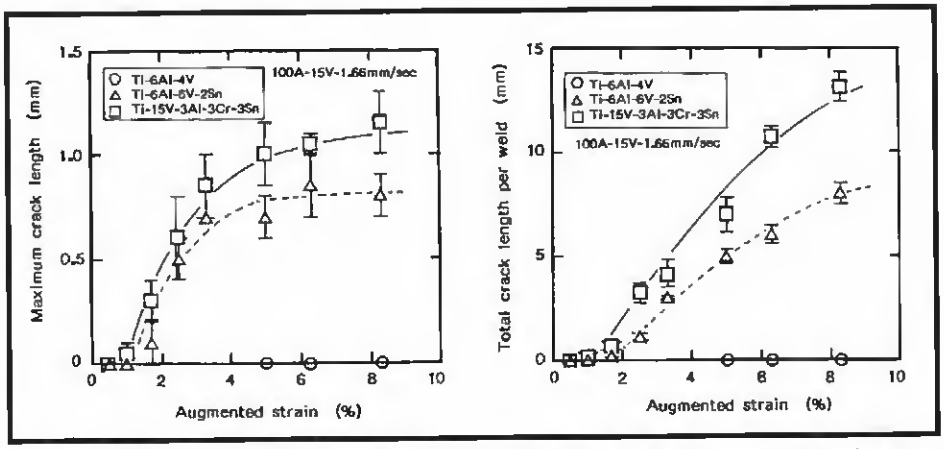

Fig. 2 — Solidification cracking susceptibility of Ti-alloys evaluated by trans-Varestraint test. A — Maximum crack length; B — total crack length.

element concentration on the surfaces was determined from the peak heights and sensitivity factors of the AES spectra on the crack surface after the Varestraint test and the ductile fracture surface after the tensile test (Ref.10). The results are listed in Table 2. In both alloys, the crack surfaces were markedly rich in V and Cr and depleted in Al and Sn. This suggests that the microsegregation of V and Cr at the dendrite boundaries on weld solidification significantly lowers the temperature at which the solidification of these alloys finishes and, in turn, leads to the formation of a continuous liquid film, which causes cracks.

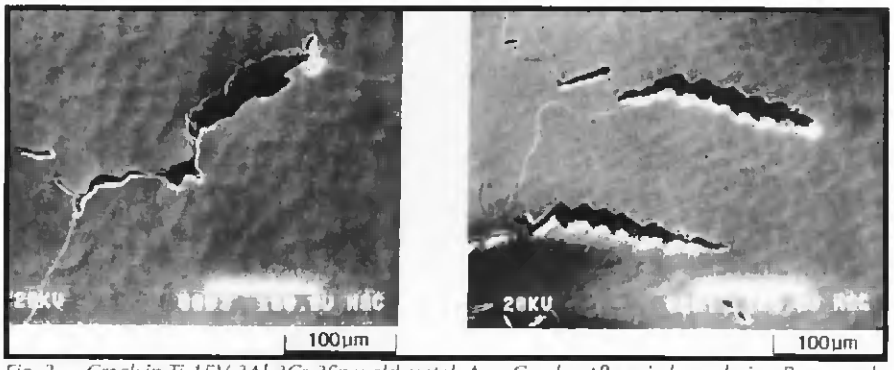

Fig. 3 — Crack in Ti-15V-3Al-3Cr-3Sn weld metal. A — Cracks at β grain boundaries; B — cracks at cellular boundaries.

Microsegregation

Figure 5 shows the solidification microstructures of the three Ti-alloy welds as exhibited by tin quenching, along with the composition profiles obtained by EPMA, the scans of which were made between A and A' approximately 100 μm away from the solidification front. Vanadium, Fe, Cr and/or Cu were enriched, while Al and/or Sn were depleted at the dendrite boundaries of each microstructure. This means that β stabilizing elements such as V, Fe, Cr and Cu were discharged into the liquid in advance of the moving solid-liquid interface on solidification. These results were consistent with those obtained by AES in Table 2, where Fe and Cu could not be confirmed, due to their small concentrations.

To determine solute element behaviors on solidification and subsequent cooling, concentration profiles of the quenched microstructures were examined using CMA. The results are shown in Figs. 6–8. The solidification fronts are to the left of the figures. The white areas are rich in the specified element, the black areas are depleted. Microsegregation was most pronounced near the solidification front of each weld metal.

Table 3 presents the distribution coefficient, k, calculated from the ratio of the element concentration in the solid to that in the liquid at the cell boundaries near the solidification front. The coefficients for Fe, Cu and Cr were fairly less than 1.0, and the difference between alloys was not significant. As presented in Fig. 6, the microsegregation of Ti-6Al-4V weld metal largely disappeared approximately 100–200 μm away from the front, while that in the other two alloys was still present in lower temperature regions, as indicated in Figs. 7 and 8.

Figure 9 depicts the changes in the Fe concentration at the dendrite boundaries, C_{db}, in tin-quenched microstructures of the three Ti-alloys. C_0 is the nominal Fe concentration. Note a significant difference in the concentration decrease of Fe between the three alloys. Any Fe microsegregation in Ti-6Al-4V weld metal diffused rapidly in the solid, and largely faded away around 400 μm, while the microsegregation in the other two alloys was still significant 400 μm from the solidification front. The Fe microsegregation in Ti-15V-3Al-3Cr-3Sn was pronounced, more than double the nominal value at 400 μm. The other elements behaved similarly to Fe.

Elemental Solid-State Diffusion

The diffusivity of Fe, which was present in all three Ti-alloys, was determined by studying diffusion welding between Ti-alloys and Type 444 ferritic stainless steel. Fe diffusion during bonding can be assumed to occur only in one direction. Since the solid-state diffusion rate of Fe in β-Ti is much larger than that of Ti in α-Fe (Refs. 11, 12), Fe diffuses from the stainless steel to the Ti alloy. The diffu-

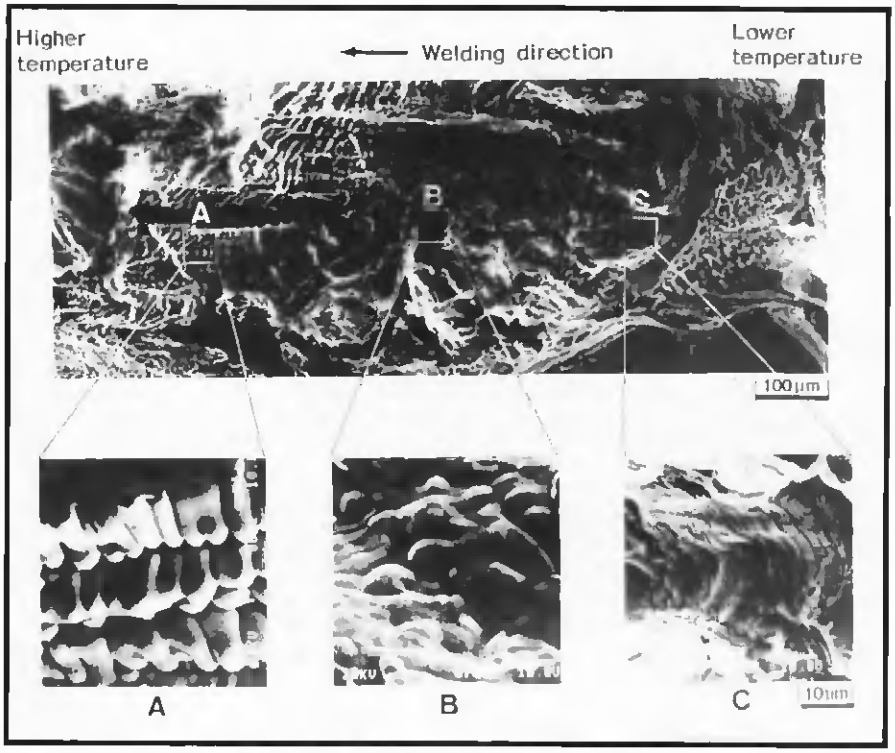

Fig. 4 — SEM microfractographs of solidification crack in Ti-15V-3Al-3Cr-3Sn weld metal.

Table 3 — The Distribution Coefficient of Solute Elements in Ti-alloys, Determined from the Difference of the Solute Concentration near the Solidification Front

Alloy	Al	V	Fe	Sn	Cu	Cr
Ti-6Al-4V	1.02	0.89	0.65	—	—	—
Ti-6Al-6V-2Sn	1.02	0.91	0.61	1.09	0.52	—
Ti-15V-3Al-3Cr-3Sn	1.08	0.95	0.71	1.13	—	0.79

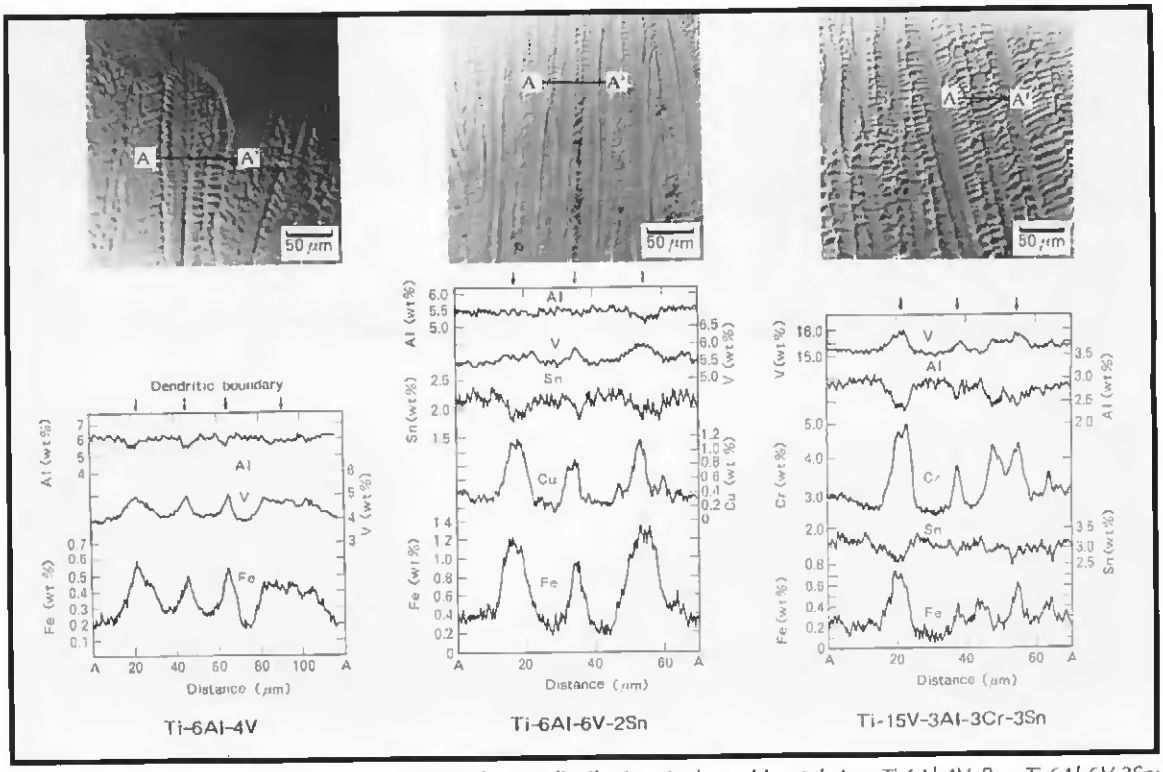

Fig. 5 — Solidification microstructures and solute element distributions in the weld metal. A — Ti-6Al-4V; B — Ti-6Al-6V-2Sn; C — Ti-15V-3Al-3Cr-35n

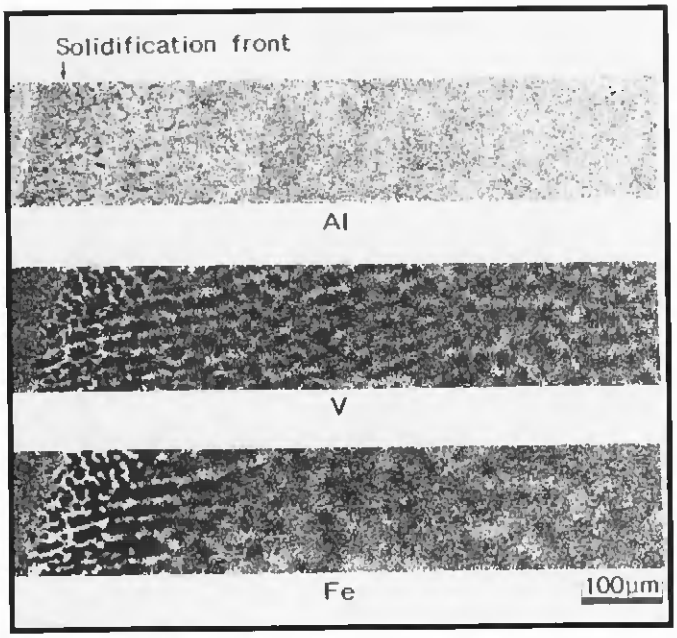

Fig. 6 — Microsegregation during solidification in the weld metal of Ti-6Al-4V. The white areas are rich in elements; the black areas are depleted.

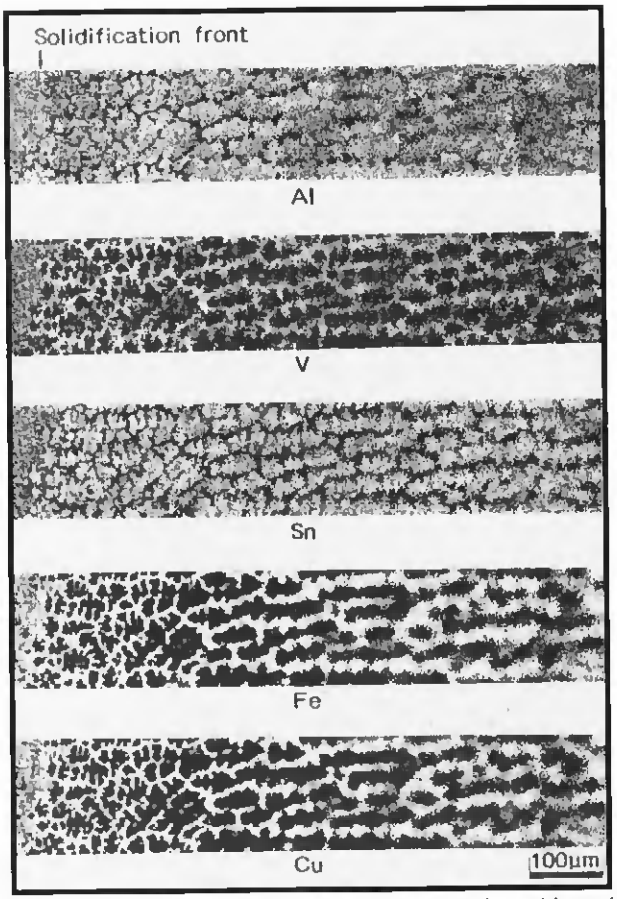

Fig. 7 — Microsegregation during solidification in the weld metal of Ti-6Al-6V-25n. The white areas are rich in elements; the black areas are depleted. A — Al; B — V; C — Sn; D — Cr; E — Fe.

sion of Fe in the Ti alloy during bonding is expressed by the following equation:

$$\partial C(x, t) / \partial t = D \, \partial^2 C(x, t) / \partial x^2 \quad (1)$$

where C is the concentration of Fe, x is the distance into the Ti-alloy from the interface, t is the bonding time and D is the diffusion coefficient of Fe in the Ti-alloy. The initial condition is given by

$$C(x, 0) = C_1 \ (x < 0) \quad (2)$$

and

$$C(x, 0) = C_0 \ (x > 0) \quad (3)$$

where C_0 and C_1 are the concentration of Fe in the Ti-alloy and the stainless steel, respectively. The boundary condition required is as follows:

$$C(0, t) = C_1 \quad (4)$$

The following equation is obtained by solving Equation 1 using the initial and boundary conditions of Equations 2–4

$$(C(x, t) - C_0)/(C_1 - C_0) = 1 - \mathrm{erf}(x/2 \cdot (Dt)^{1/2}) \quad (5)$$

where erf(z) is the error function.

Table 4 — Constants Used for Calculation of Fe Microsegregation during Solidification

	Ti-6Al-4V	Ti-6Al-6V-2Sn	Ti-15V-3Al-3Cr-3Sn
Nominal composition (Co) (wt-%)	0.22	0.75	0.21
Dendrite arm spacing (d) (mm)	2×10^{-2}	2×10^{-2}	2×10^{-2}
Diffusion coefficient in solid (D_s) (m^2/s)	2.5×10^{-10}	4.9×10^{-11}	3.5×10^{-11}
Local solidification time (t_f) (s)	0.06	0.12	0.10
Equilibrium distribution coefficient (k)	0.65	0.61	0.71

t_f: Local solidification time.
d: Dendrite arm spacing.

Figure 10 gives the diffusion coefficients of Fe in the Ti-alloys, which were determined from the measured Fe concentration and Equation 5. All diffusion welding was performed below 1358 K, because at and above this temperature Fe and Ti eutectic constituents would be formed (Ref. 13). Diffusion coefficients at higher temperatures were extrapolated from these data. As seen in Fig.10, the diffusion coefficient of Fe in Ti-6Al-4V was similar to that in pure Ti, as found in earlier studies (Ref. 12). Diffusion coefficients in the other Ti-alloys were much less than those, which presumably caused the delay of solute homogenization. The measured Fe concentration curves in Fig. 9 were also confirmed by the diffusion calculation, using the obtained Fe diffusion rates in Fig. 10. In general, Fe easily diffuses interstitially into the β-Ti matrix (Refs. 14, 16). In the Ti-alloys containing Sn, Cr and Cu, however, Fe is liable to form microcomplex clusters or compounds with these additional elements. This might eventually lower the diffusion rate of Fe and additional elements themselves (Refs.14–16), even that of V and Al. A similar mechanism has been observed in the diffusion

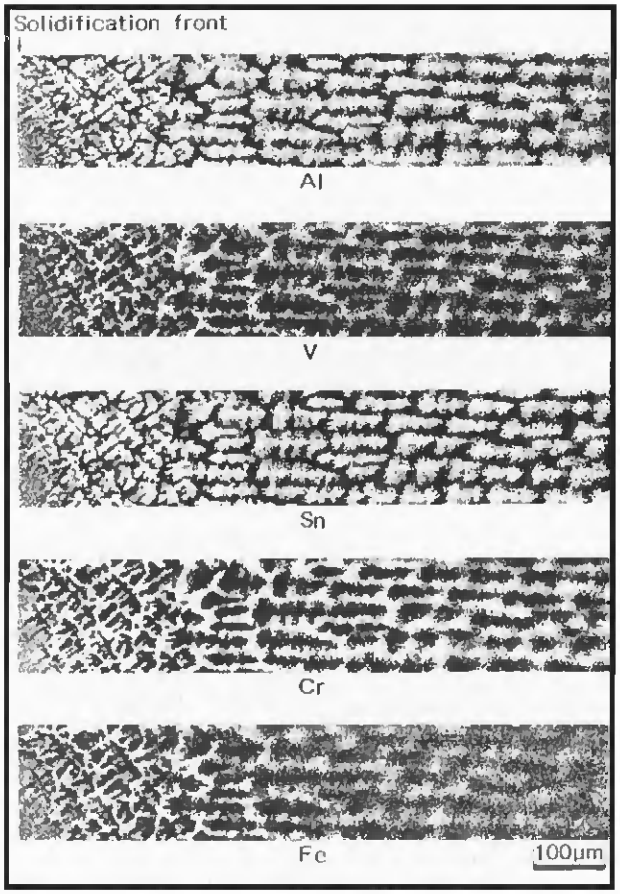

Fig. 8 — Microsegregation during solidification in the weld metal of Ti-15V-3Al-3Cr-3Sn. The white areas are rich in elements; the black areas are depleted. A — Al; B — V; C — Sn; D — Cr; E — Fe.

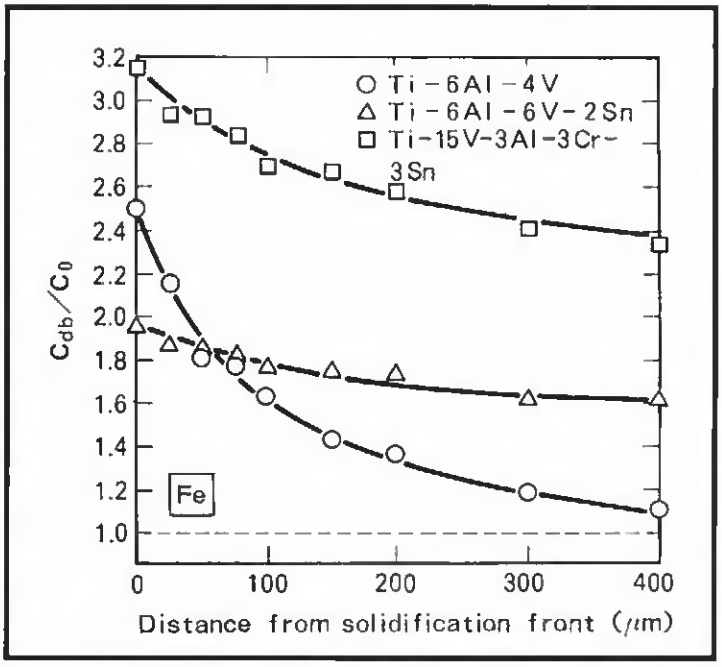

Fig. 9 — Changes in Fe concentration measured at dendrite boundaries in tin-quenched microstructures of three different Ti-alloy welds exhibited in Figs. 6–8. Horizontal axis shows the distance from the solidification front. C_{db}: Fe concentration at dendrite boundaries; C_0: nominal composition.

of Ni in Pb-Cd alloys (Refs. 14, 15).

The microsegregation of Fe during solidification was calculated using the diffusion and distribution coefficients obtained above. When the local equilibrium at the liquid-solid interface, complete mixing in the liquid, and limited diffusion in the solid are assumed, the solute concentration, C_s, of the solid at the liquid-solid interface is given by the following equations (Ref. 17):

$$C_s = kC_0(1 - f_s / (1-ak))^{k-1} \quad (6)$$

$$a = 4D_s t_f / d^2 \quad (7)$$

where k is the equilibrium distribution coefficient, C_0 is the nominal solute concentration and f_s is the fraction solid. D_s, t_f and d are the diffusion coefficient in the solid, the local solidification time, and the dendrite arm spacing, respectively. Figure 11 gives the concentration profile of Fe in the solid (C_s/C_0) in each alloy calculated using the constants indicated in Table 4. From CMA results and the welding velocity, d and t_f were determined. Although there were hardly differences between the distribution coefficients of Fe in the three alloys, the concentration of Fe at the terminal solidification stage in Ti-6Al-6V-2Sn and Ti-15V-3Al-3Cr-3Sn was much larger than that in Ti-6Al-4V. This means that the effect of the Fe back-diffusion in the solid during solidification on the microsegregation of Ti-alloy weld metals was profound. As shown in Figs. 7 and 8, the other solute microsegregation at the solidification front in Ti-6Al-6V-2Sn and Ti-15V-3Al-3Cr-3Sn welds was remarkable as well, and the homogenization after solidification was also considerably delayed. This indicates that the solute diffusion rates in the solid were small in these two alloys. Note that the solute back-diffusion in the solid during solidification was small in these two alloys, *i.e.*, the effect of the solid-state back-diffusion of solutes on the microsegregation was significantly different from that in Ti-6Al-4V.

Solidification Cracking Mechanism

In Ti-6Al-4V weld metal, the microsegregation of V and Fe at the dendrite boundaries during solidification was not significant, diffusing readily in the solid. This means that the solidification temperature range between onset and completion of the solidification was narrow due to the large back-diffusion of solute elements in the solid during solidification. On the other hand, in Ti-6Al-6V-2Sn and Ti-15V-3Al-3Cr-3Sn weld metal, the microsegregation of V, Fe, Cu and/or Cr at the dendrite boundaries during solidification was marked, hardly diffusing in the solid. Hence, the solidification temperature range should be large because of the much smaller back-diffusion of solute elements in the solid during solidification. That would lead to formation of a residual low melting liquid film, resulting in solidification cracking (Ref.9).

Conclusions

1) According to the trans-Varestraint test, Ti-6Al-4V weld metal did not crack at all, while cracking occurred above 0.5% augmented strain in welds of Ti-6Al-6V-2Sn and Ti-15V-3Al-3Cr-3Sn. The latter alloy was the most susceptible

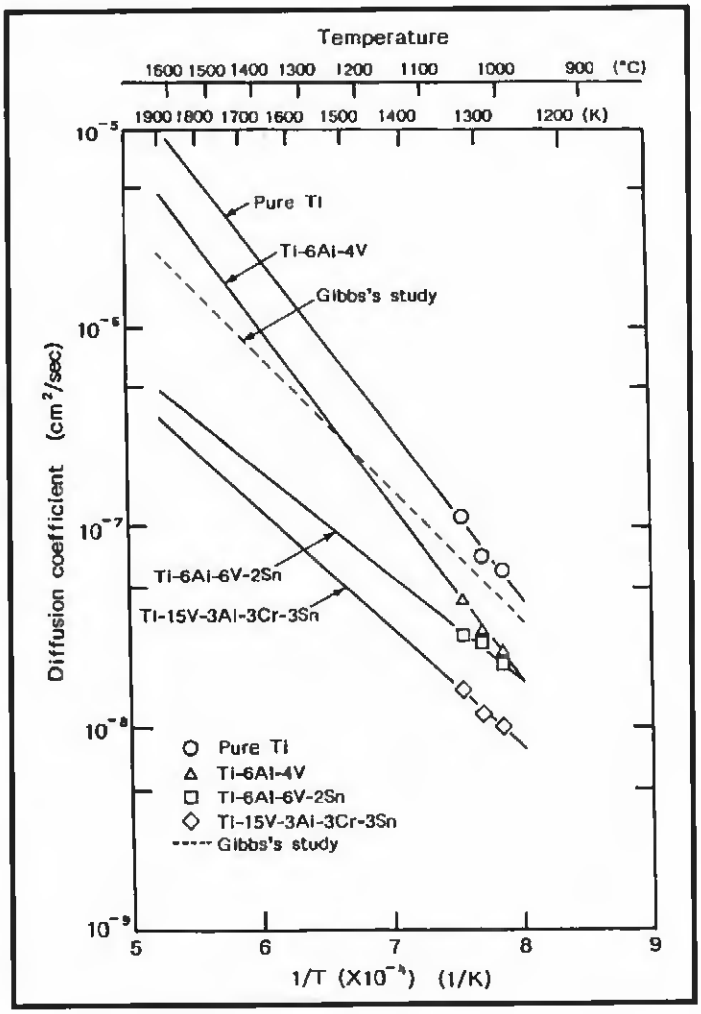

Fig. 10 — Diffusion coefficient of Fe in Ti-alloys, determined by the diffusion welding experiment.

Fig. 11 — Effect of the solid-state back-diffusion on Fe microsegregation during weld solidification.

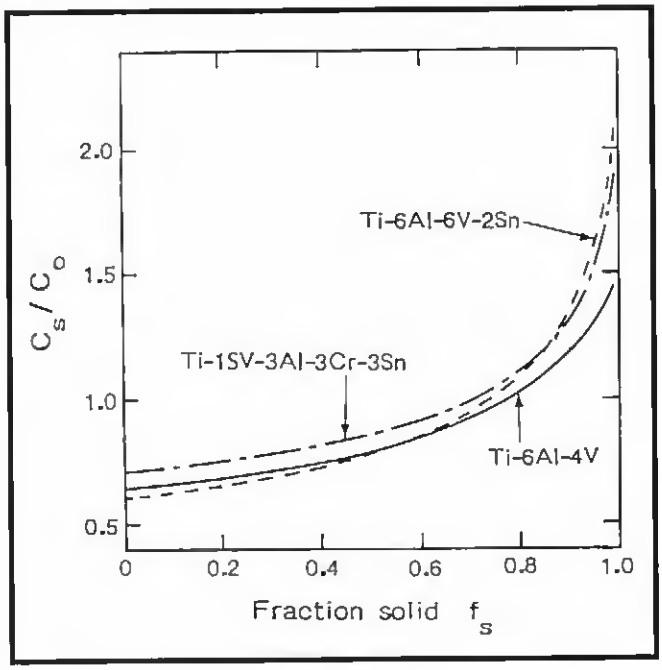

to cracking. The crack surfaces exhibited the smooth appearance of dendritic structures, and indicated a clear vestige of residual liquid film.

2) At the dendrite boundaries of the solidification microstructures, V, Fe, Cr and/or Cu were enriched, while Al and/or Sn were depleted. The distribution coefficients of Fe, Cr and Cu on solidification were fairly less than 1.0, resulting in solute enrichment at the solidifying dendrite cell boundaries.

3) Solute microsegregation occurring in Ti-6Al-4V during solidification was not significant due to the large solute back-diffusion in the solid. After solidification there was a rapid dispersion in the matrix and a homogenization at an early stage of weld cooling. Solute microsegregation of the other two alloys during solidification was more noticeable due to the much smaller back-diffusion of solute elements in the solid. After solidification there was hardly any diffusion in the matrix, and thus it largely remained at ambient temperature.

4) The solidification temperature range of Ti-6Al-6V-2Sn and Ti-15V-3Al-3Cr-3Sn weld metals should be wide due to the much smaller back-diffusion of solute elements in the solid during solidification, which could lead to formation of a residual liquid film of low melting constituents, resulting in cracks.

Acknowledgments

One of the authors, T. Ogawa, would like to acknowledge Andrew Garner and the Pulp and Paper Research Institute of Canada for support during his sabbatical when this manuscript was drafted.

References

1. Prokhorov, N. N. 1986. Hot cracking resistance of Ti-alloys in welding. *Welding Production* 33(9):40–42.

2. Baeslack III, W. A. 1980. Observations of solidification cracking in Ti-alloy weldments. *Metallography* 13:277–281.

3. Hayduk, D., Damkroger, B. K., Edwards, C. R., and Olson, D. L. 1986. Cracking susceptibility of Ti-6Al-2Nb-1Ta-0.8Mo as determined by the Varestraint test. *Welding Journal* 65:251-s to 260-s.

4. Baeslack III, W. A., Becker, D. W., and Froes, F. H. 1984. Advance in Ti-alloy welding metallurgy. *Journal of Metals* 36(5):46–58.

5. Hemsworth, B., Bonizewski, T., and Eator, N. F. 1969. Classification and definition of high temperature welding cracks in alloys. *Metal. Const. and Brit. Weld. J.* 2:5-s to 16-s.

6. Kujanpaa, V. P., David, S. A., and White, C. L. 1986. Formation of hot cracks in austenitic stainless steel welds — solidification cracking. *Welding Journal*, 65:203-s to 212-s.

7. Cieslak, M. J., and Savage, W. F. 1985. Hot cracking studies of alloy CN-7M. *Welding Journal* 64:119-s to 126-s.

8. Arata, Y., Matsuda, F., and Nakata, K. 1975. Effect of solidification rate on solidification structure in weld metal. *Journal of High Temperature Society* 1:160–168 (in Japanese).

9. Weiss, B., Grotke, G. E., and Stickler, R. 1970. Physical metallurgy of hot ductility testing. *Welding Journal* 49:471-s to 487-s.

10. *Handbook of Auger Electron Spectroscopy* (P.E.D.), p. 4.

11. *Metal Data Book*, 2nd edition, 1984. The Japan Institute of Metal, Maruzen, Japan, p. 28 (in Japanese).

12. Gibbs, G. B., Graham, D., and Tomlin, D. H. 1963. Diffusion in Ti and Ti-Nb alloys. *The Philosophical Magazine* 8:1269–1282.

13. Murray, J. L. 1981. The Fe-Ti system. Bulletin of alloy phase diagram 2(3):320–334.

14. Warburton, W. K., and Turnbull, D. 1975. *Diffusion in Solid.* Academic Press, p. 171.

15. Nakajima, H. 1981. Diffusion of nickel in lead-cadmium alloy. *Scripta Metallurgica* 15:577–580.

16. Nakajima, H. 1983. Fast diffusion of impurity in a few kinds of metal. Bulletin of The Japan Institute of Metal 22:480-487 (in Japanese).

17. Flemings, M. C. 1974. *Solidification Processing.* McGraw-Hill, p. 145.